Journal of Applied Chemistry
JAC
http://chemistry.journals.semnan.ac.ir

Ethylenediaminetetraacetic acid coated Fe_3O_4@SiO_2 nanocomposite: An effective adsorbent for the removal of copper ions from aqueous solutions

Mohsen Esmaeilpour*, Afsanehsadat Larimi, Majid Ghahramanafshar, Morteza Faghihi

Chemical and Process Engineering Department, Niroo research Institute, Tehran, Iran

Article history:
Received: 11/Dec/2021
Received in revised form: 15/Mar/2022
Accepted: 04/May/2022

Abstract

A novel ethylenediaminetetraacetic acid (EDTA) supported on Fe_3O_4@SiO_2 nanocomposite with a core-shell structure was developed, aiming to remove of copper ions from aqueous media. During the first step, Fe_3O_4@SiO_2 nanosphere core-shell is synthesized using nano-Fe_3O_4 as the core, TEOS as the silica source and PVA as the surfactant. Then, Fe_3O_4@SiO_2 was coated with ethylenediaminetetraacetic acid. The properties of surface functional groups, crystal structure, magnetism and surface morphology of magnetic nanoparticles were characterized by Fourier transform infrared spectroscopy (FT-IR), X-ray diffraction (XRD), transmission electron microscopy (TEM), field emission scanning electron microscopy (FE-SEM), dynamic light scattering (DLS) and vibration sample magnetometry (VSM). The effect of parameters influencing adsorption efficiency including adsorbent dosage and contact time of adsorbent on the sorption behavior was assessed and discussed. The adsorption kinetics studies of the novel adsorbent in removing copper ions from waste water showed that the maximum absorption amounts of Cu(Π) were 95% at 25ºC. Desorption and reusability of Fe_3O_4@SiO_2-EDTA was also investigated for tested copper ions based on sequential adsorption desorption cycles. Therefore, all the studied results indicated that Fe_3O_4@SiO_2-EDTA nanocomposites were an efficient and reusable adsorbent for removal of copper ions from aqueous solutions.

Keywords: Fe_3O_4@SiO_2 nanocomposite, Surface modification, Ethylenediaminetetraacetic acid, Copper ions, Removal efficiency, Adsorption kinetics.

1. Introduction

Heavy metal ions and dyes from industrial wastes pose threat to the environment and human health, therefore their quantitative removal and a constant monitoring of their concentration are important issues. Although some of them are fundamental for human metabolism and are well known as dietary minerals, all of them are potentially toxic at higher concentrations [1-3].

*.**Corresponding author:** Assistant Professor of Chemistry, Niroo Research Institute, Chemical and Process Engineering Department, Tehran, Iran. *E-mail address: Mesmaeilpour@nri.ac.ir*

Numerous approaches such as biological processes and physical chemical including adsorption, ion-exchange, precipitation, biosorption, reverse osmosis, filtration and other membrane separations have been widely used to purify water containing excessive amounts of heavy metal ions [4]. It is well-known that copper compounds are widely used in many industrial processes, such as the wood pulp production, electric devices, antifouling paints, manufacturing of fungicides, metal plating, and so on [5]. The industrial waste effluents contain a large amount of copper pollutants, which are harmful to ecological systems and human health. It has been reported that ingestion of copper at certain amount is responsible for kidney or liver damage, intestinal disorders, temporary stomach and even cancer [6, 7]. Therefore, adsorption technique has received much attention because it allows the use of many materials that are environmental friendly and have low production cost [8, 9]. Effectiveness even to remove trace amount of heavy metal ions present in aqueous phase is the major merit of adsorption process [10]. In addition, it is an important process to understand the accumulation of heavy metal ions at lignite, plant wastes, activated carbon, carbon nano-tubes, clay minerals, solid-solution interfaces and nano-graphite encapsulated alginate beads have been widely investigated adsorbents for the removal of heavy metal ions from aqueous solution and wastewater [11, 12].

Iron oxides in the nano range, have been extensively considered as a fascinating class of materials from the viewpoints of both theory and practical applications, which exhibit tremendous potential in magnetic resonance imaging, gas sensors, bioseparation, catalytic materials, ion exchangers, magnetic recording devices, adsorbents for water purification, etc [13, 14]. Among nano-iron oxides, Fe_3O_4 magnetic nanoparticles (MNPs) are gaining growing attention by researchers from diverse fields due to their unique physical properties such as low toxicity, small size, high magnetic saturation, higher surface area and a simple preparation process by a magnetic field [15,16]. However, iron oxide activity is affected by its trends to be aggregated that can block their applications easily [17, 18]. In addition, when Fe_3O_4 nanoparticles exposed to atmosphere, they could be oxidized due to their fewer activating groups [19-21]. The acidic conditions is also harmful for magnetite particles because they are susceptible to leaching under these conditions [22, 23]. Therefore, using stabilizers as the shell is vital to control their size increases. Among stabilizers, coating with a silica layer as the stabilizer, which prevents direct contact between the nanoparticles has attracted great attention in recent years.

Furthermore, the abound hydroxyl groups on the surface of silica layer provide the opportunity to conjugate various function molecules for many special applications [24, 25].

Therefore, in this paper, we report on our preparation and characterization of Fe_3O_4@SiO_2 nanoparticles modified with ethylenediaminetetraacetic acid (Fe_3O_4@SiO_2-EDTA) (**Figure 1**). Then, we have investigated the adsorbent dosage on the adsorption and the uptake capacity as a function of contact time (adsorption kinetics) for the removal of copper ions from aqueous system.

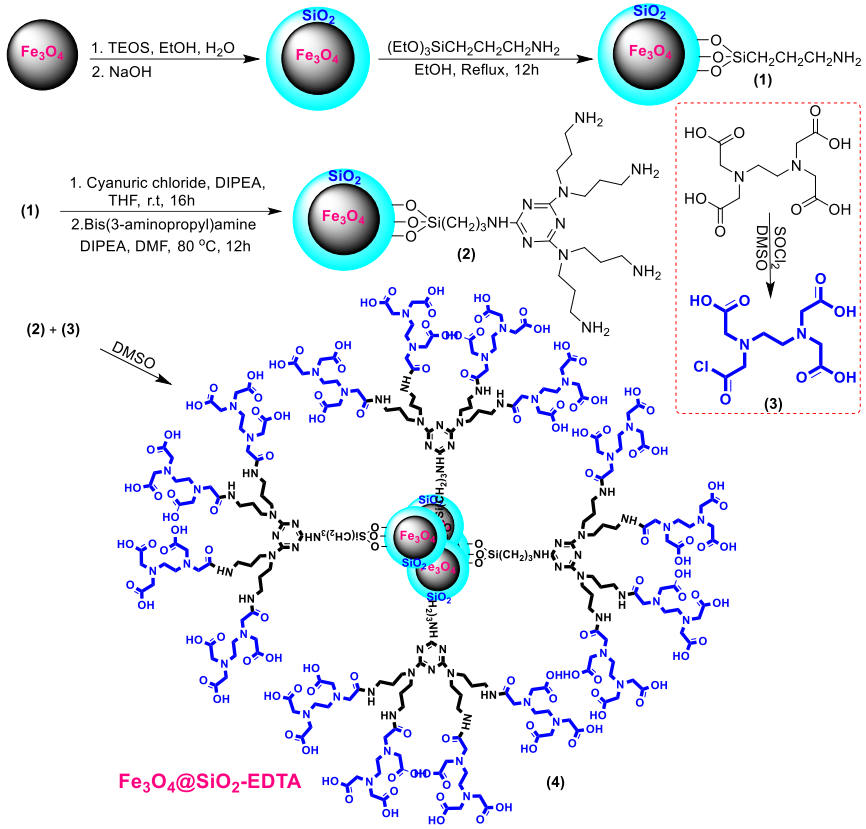

Figure 1. Schematic representation of the synthesis of Fe_3O_4@SiO_2-EDTA NPs.

2. Experimental procedure

2. 1 Materials and method

Reagents and solvents were obtained from commercial suppliers and used without further purification. Fourier transform infrared (FT-IR) spectra were run on a Shimadzu FTIR-8300 spectrophotometer and the sample and KBr were pressed to form a tablet. The powder XRD patterns were recorded on a Bruker AXS D8-advance X-ray diffractometer using a Cu Kα radiation (λ= 1.5418). Field emission scanning electron microscopy (FE-SEM) was obtained using a Hitachi S-4160 electron microscope. The particle size and morphology were investigated by a Philips EM208 microscope on an accelerating voltage of 100 kV. The hydrodynamic size of the MNPs was determined by dynamic light scattering (DLS) using a HORIBA-LB550. The magnetic behavior of the samples was conducted on Lake Shore vibrating sample magnetometer (VSM) at room temperature. The metal concentrations were measured with an inductively coupled plasma spectrometer (ICP, analysis (Varian, Vista-pro). The amount of copper ions adsorbed on the magnetic adsorbents was calculated from a mass balance.

2. 2 Preparation of Fe_3O_4@SiO_2 core-shell

The Fe_3O_4 nanoparticles were synthesized by a facile coprecipitation method [26]. Briefly, $FeCl_3.6H_2O$ (1.3 g, 4.8 mmol) was dissolved in 30 ml of water, followed by addition of poly(vinyl alcohol) (PVA 15000, 1 g) as a surfactant and 0.9 g (4.5 mmol) of $FeCl_2.4H_2O$. The mixture was stirred vigorously for 30 min at 80 °C. Then, to this mixture, hexamethylenetetramine (1.0 mol/L) was slowly added under vigorous stirring to produce a black precipitate and the solution pH was maintained at 10.0. The resultant mixture was continuously stirred with nitrogen protection at 60 °C for 2 h and the obtained black magnetite particles were collected with a permanent magnet, and sequentially washed with ethanol and dried at 80 °C for 10 h. Fe_3O_4@SiO_2 core-shell nanospheres were prepared through a modified Stöber method [27]. In a typical process, 0.5 g of Fe_3O_4 nanoparticles were dispersed in a mixture of ethanol (50 mL), deionized water (5 mL) and 5.0 ml of NaOH (10 wt.%). Subsequently, 0.2 mL of tetraethoxysilane (TEOS) was added dropwise under vigorous mechanical stirring. After stirring for 30 min, the products (Fe_3O_4@SiO_2) were

collected using an external magnet and washed with deionized water and ethanol three times and then dried under vacuum at 80 °C for 10 h.

2.3. Preparation of Fe_3O_4@SiO_2-NH_2 MNPs

To a suspension of SiO_2-coated magnetite particles (1 g) in ethanol (10 mL), 3-amino propyl(triethoxy)silane (1 mmol, 0.25 mL) was added. The mixture was refluxed for 12 h, and then, it was cooled to room temperature to obtain a brown precipitate. The obtained solid was separated with an external magnet, washed with water and ethanol (1:1) to remove unreacted species, and dried under vacuum at 80 °C [28].

2.4. Preparation of cyanuric chloride functionalized Fe_3O_4@SiO_2-NH_2 MNPs (Fe_3O_4@SiO_2-TCT)

Modification of Fe_3O_4@SiO_2-NH_2 nanoparticles with cyanuric chloride (TCT) was achieved by introducing TCT (1.0 mmol, 0.185 g) and diisopropylethylamine (DIPEA) (1 mmol, 0.17 mL) into the THF (10 mL) suspension of Fe_3O_4@SiO_2-NH_2 (1 g) nanoparticles under stirring. The mixture was stirred for 12 h at room temperature. The resultant Fe_3O_4@SiO_2-TCT nanoparticles were separated by a magnetic device and washed with hot ethanol several times to completely remove un-adsorbed components and dried at 60 °C for 8 h [28].

2.5. Preparation of Fe_3O_4@SiO_2-TCT-NH_2 MNPs

Bis(3-aminopropyl)amine (16 mmol, 2.0 mL) and DIPEA (16 mmol, 2.8 mL) were added into the dispersion of Fe_3O_4@SiO_2-TCT NPs (1 g) in DMF (20 mL). Then, the dispersed mixture was ultrasonicated for 10 min and stirred at 80 °C for 12 h. The resulting Fe_3O_4@SiO_2-TCT-NH_2 NPs was separated with a magnet and washed with deionized water and hot ethanol successively, and finally dried for 4 h at 70 °C [28].

2.6. Preparation of Fe_3O_4@SiO_2-EDTA NPs

To conjugate EDTA to Fe_3O_4@SiO_2-TCT-NH_2, first, EDTA (2 mmol) was mixed with 20 mL of DMSO and thionyl chloride ($SOCl_2$) (2 mmol) was then slowly added to the mixture through a constant pressure drop funnel. Immediately after the $SOCl_2$ was completely dropped, 1.5 g of Fe_3O_4@SiO_2-TCT-NH_2 was quickly added to the mixture. The mixture was stirred at room temperature for 2 h. Finally, the Fe_3O_4@SiO_2-EDTA NPs were separated with a magnet and washed with acetone, sodium carbonate solution (0.1 mol L^{-1}) and deionized water and dried at 60 °C [28].

3. Results and discussion

3.1. Characterization of EDTA functionalized Fe_3O_4@SiO_2 NPs

Ethylenediaminetetraacetic acid functionalized Fe_3O_4@SiO_2 NPs was prepared (**Figure 1**), then characterized with some analyses including FTIR, XRD, TEM, FE-SEM, DLS and VSM.

Figure 2 shows the FT-IR spectra of Fe_3O_4, Fe_3O_4@SiO_2, Fe_3O_4@SiO_2-NH_2, Fe_3O_4@SiO_2-TCT, Fe_3O_4@SiO_2-TCT-NH_2, Fe_3O_4@SiO_2-EDTA MNPs. The FT-IR spectra (**Figure 2a**) revealed that the as-made Fe_3O_4 microspheres displayed a vibration band at 570 cm^{-1}, which is indicative of the typical Fe-O bond [29]. The Fe_3O_4@SiO_2 sample showed new broad peaks at 1090 and 792 cm^{-1}, which were attributed to the stretching bonds of Si-O-Si [30], suggesting the successful coating of a thin silica layer on the Fe_3O_4 surface (**Figure 2b**). The presence of 3-amino propyl(triethoxy)silane on the nanoparticle surface was confirmed by the absorbance peaks at 576 (Fe-O), 1123 (Si-O-Si), 2810-2986 (C-H) and 3303-3351 cm^{-1} (Figure 2c). Comparison of the spectrum of Fe_3O_4@SiO_2-NH_2 with Fe_3O_4@SiO_2-TCT composite NPs shows characteristic absorption bands at 576, 1091 and 2866-2992 cm^{-1} and also adsorption peaks of cyanuric chloride at 1511, 1564 and 1711 cm^{-1}. This indicates that cyanuric chloride moieties are supported on Fe_3O_4@SiO_2-NH_2 NPs (**Figure 2d**) [31]. The FT-IR spectrum of Fe_3O_4@SiO_2-TCT-NH_2 (**Figure 2e**) showed new peaks at 2871-3057, 1451 and 1257 cm^{-1} that are attributed to C-H (symmetric and asymmetric stretching vibrations), CH_2 (bending) and C-N (stretching vibration), respectively (**Figure 2e**). In the FT-IR spectra of Fe_3O_4@SiO_2-EDTA (**Figure 2f**), basic characteristic vibrations of C-H bands (asymmetric and symmetric stretching) at 2885-3070 cm^{-1}, Si-O-Si asymmetric stretching and symmetric stretching at 1095 and 801 cm^{-1} and the stretching vibration of Fe-O were observed at 578 cm^{-1}. Furthermore, the characteristic bands of the

carbonyl groups were observed at 1736 cm^{-1} (C=O carboxylic acid stretching vibration) and 1629 cm^{-1} (C=O amide stretching vibration).

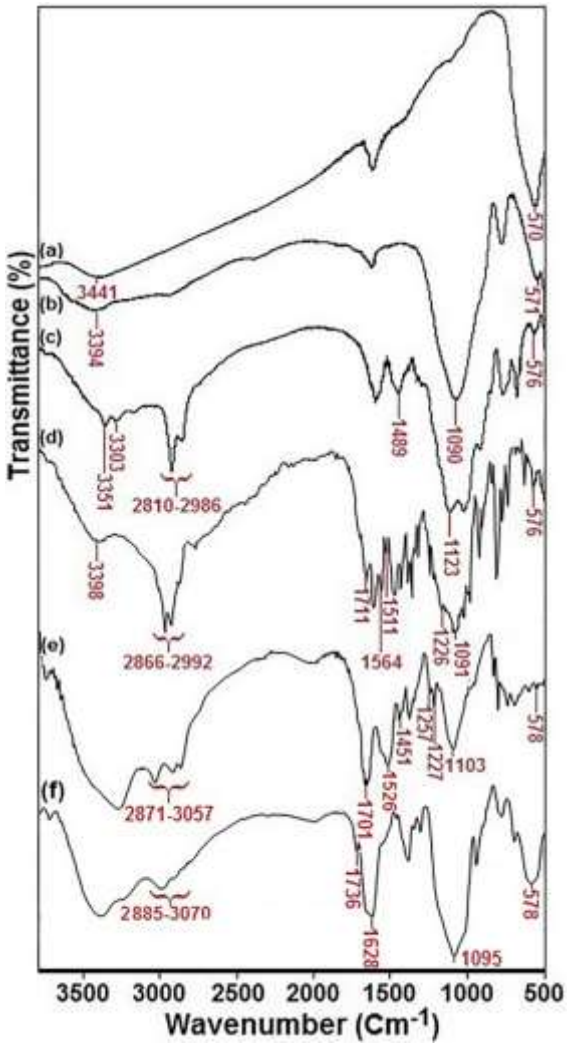

Figure 2. FTIR spectra of (a) Fe_3O_4, (b) Fe_3O_4@SiO_2, (c) Fe_3O_4@SiO_2-NH_2, (d) Fe_3O_4@SiO_2-TCT, (e) Fe_3O_4@SiO_2-TCT-NH_2 and (f) Fe_3O_4@SiO_2-EDTA NPs.

The XRD patterns for Fe_3O_4, Fe_3O_4@SiO_2 and Fe_3O_4@SiO_2-EDTA nanocomposites exhibited the similar pattern with respect to MNPs as shown in **Figure 3**. All diffraction peaks at 2Θ= 30.1°, 35.4°, 43.1°, 53.4°, 57.0° and 62.6° for Fe_3O_4@SiO_2 and Fe_3O_4@SiO_2-EDTA nanoparticles were also observed, which are in agreement with the XRD peaks of pure Fe_3O_4 nanoparticles [32, 33]. These peaks corresponded to (220), (311), (400), (422), (511) and (440) reflection of Fe_3O_4, respectively, indicating that the Fe_3O_4@SiO_2 and Fe_3O_4@SiO_2-EDTA NPs did not result in the crystallinity change of Fe_3O_4 nanospheres [34-36]. Furthermore, the patterns of Fe_3O_4@SiO_2 and Fe_3O_4@SiO_2-EDTA show an obvious diffusion peak around 2θ= 10-25° attributable to amorphous silica (**Figure 3b** and **c**). For Fe_3O_4@SiO_2-EDTA NPs, the broad peak is transferred to lower angles due to the synergetic effect of amorphous silica and ligand (**Figure 3c**).

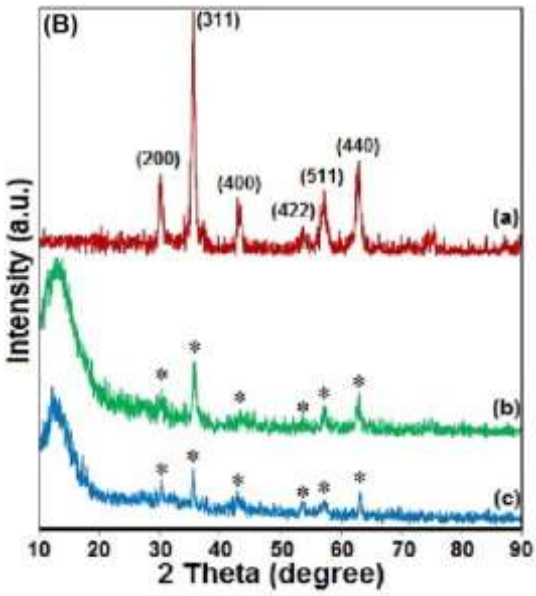

Figure 3. XRD patterns: (a) Fe_3O_4; (b) Fe_3O_4@SiO_2; (c) Fe_3O_4@SiO_2-EDTA nanocomposites.

TEM, FE-SEM and DLS images of the nanoparticels have been represented in **Figure 4**. **Figure 4a-d** shows TEM and FE-SEM images of Fe_3O_4 and Fe_3O_4@SiO_2, respectively. The size of nanoparticles obtained from the TEM images, which shows 10 and 20 nm for Fe_3O_4 and Fe_3O_4@SiO_2, respectively, and FE-SEM images shows their shapes are nearly spherical (**Figure 4a, b**). **Figure** 4e show FE-SEM images of Fe_3O_4@SiO_2-EDTA NPs. As it is shown, these nanoparticles have spherical shapes with approximately 30 nm diameters. To investigate the size distribution of these nanoparticles, particle size histograms were prepared for Fe_3O_4, Fe_3O_4@SiO_2 and Fe_3O_4@SiO_2-EDTA (**Figure 4f-h**), respectively by DLS analysis. This size

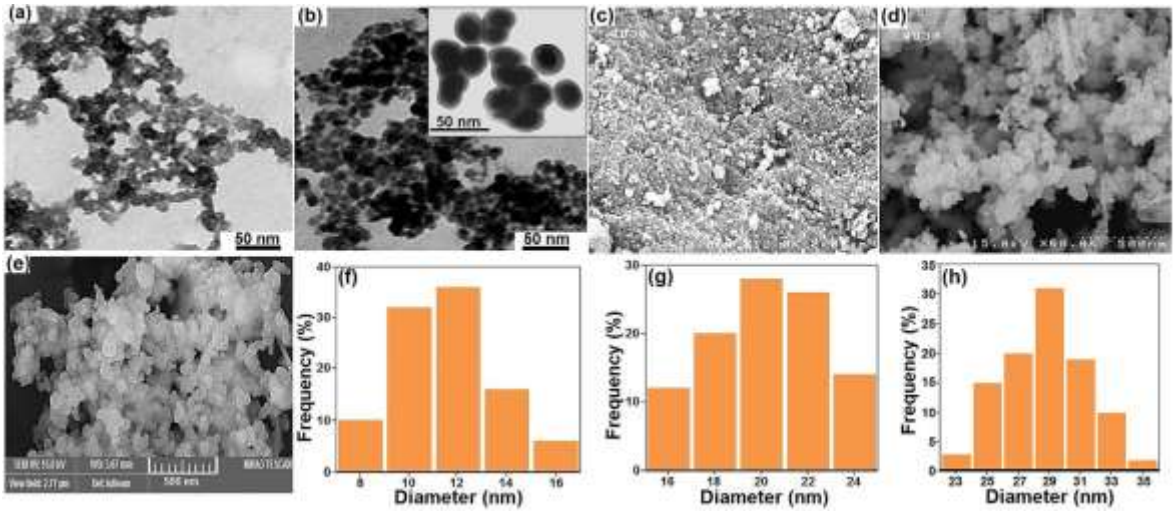

Figure 4. TEM images of a) Fe_3O_4 and b) Fe_3O_4@SiO_2; FE-SEM images of c) Fe_3O_4, e) Fe_3O_4@SiO_2, d) Fe_3O_4@SiO_2-EDTA and the size distributions of e) Fe_3O_4, f) Fe_3O_4@SiO_2 and g) Fe_3O_4@SiO_2-EDTA, respectively.

distribution is centered at a value of 12, 20, 35 and 29 nm for Fe_3O_4, Fe_3O_4@SiO_2 and Fe_3O_4@SiO_2-EDTA NPs, respectively.

The magnetic properties of the solids Fe_3O_4, Fe_3O_4@SiO_2 and Fe_3O_4@SiO_2-EDTA NPs were investigated in **Figure 5**. The curves show no remnant magnetization or coercivity, indicating that all samples are superparamagnetic at room temperature. The solid Fe_3O_4 of saturation magnetization was 64.8 emu/g (**Figure 5Aa**). The core-shell NPs (Fe_3O_4@SiO_2) presented a saturation magnetization 40.3 emu/g (**Figure 5Ab**) and EDTA-modified Fe_3O_4@SiO_2 nanospheres (Fe_3O_4@SiO_2-EDTA) presented a saturation magnetization 33.6 emu/g, respectively (**Figure 5Ac**). These results indicated that the magnetization of Fe_3O_4 decreased considerably with the increase of SiO_2 and organic molecules. Nevertheless, ethylenediaminetetraacetic acid (EDTA)-coated Fe_3O_4@SiO_2 magnetic nanocomposite can still be separated from the solution by using an external magnetic field on the sidewall of the reactor (**Figure 5B**).

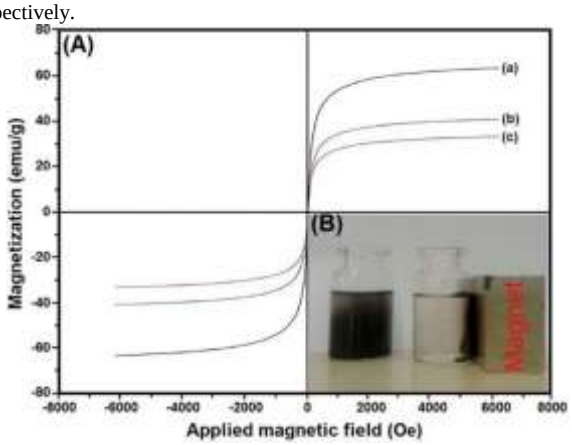

Figure 5. A) VSM curves for a) Fe_3O_4, b) Fe_3O_4@SiO_2 and c) Fe_3O_4@SiO_2-EDTA NPs; B) Magnetic recovery of the nanoparticles (inserted image).

3.2. Effect of adsorbent dosage on Cu(II) ions adsorption

The adsorbent dosage of 2, 4, 6, 8, and 10 mg in 50 mL of solution was investigated at 25 ºC for Cu(II) adsorption. As shown in **Figure 6a**, the more dosage of magnetic Fe_3O_4@SiO_2-EDTA (from 2 to 8 mg), the higher uptake capacity can be reached; but the higher amounts of adsorbent did not improve the adsorption (10 mg). As a result, we found 8 mg of Fe_3O_4@SiO_2-EDTA MNPs in 50 mL of solution as the optimum amount for the adsorption approach.

3.3. Adsorption kinetics

The time-dependent behavior of metal(II) ions adsorption onto Fe_3O_4@SiO_2-EDTA MNPs (8 mg) containing 50 mL Cu(II) solution was evaluated for different equilibrium time intervals from 2.5 to 15 min at 25 ºC by using initial concentration of 0.2 mmol/L for Cu(II). The magnetic adsorbent nananoparticles were removed with a magnet

and the resultant solutions were analyzed for metal ions using ICP. **Figure 6b** shows clearly the adsorption of Cu(II) on Fe_3O_4@SiO_2-EDTA as a function of contact time. The adsorption amount of Cu(II) is evidently increased with the enhancement of contact time up to 12.5 min. It seems that the presence of many active sites on the Fe_3O_4@SiO_2-EDTA MNPs surface and also the prompt diffusion of the ions through the boundary surface at the liquid-solid interface are the main reasons for which. Also, the adsorption kinetics show that pseudo-second-order kinetic model provides a better correlation as compared to pseudo-first-order kinetic model for the adsorption of of Cu(II) ions onto ethylenediaminetetraacetic acid coated Fe_3O_4@SiO_2 nanocomposite.

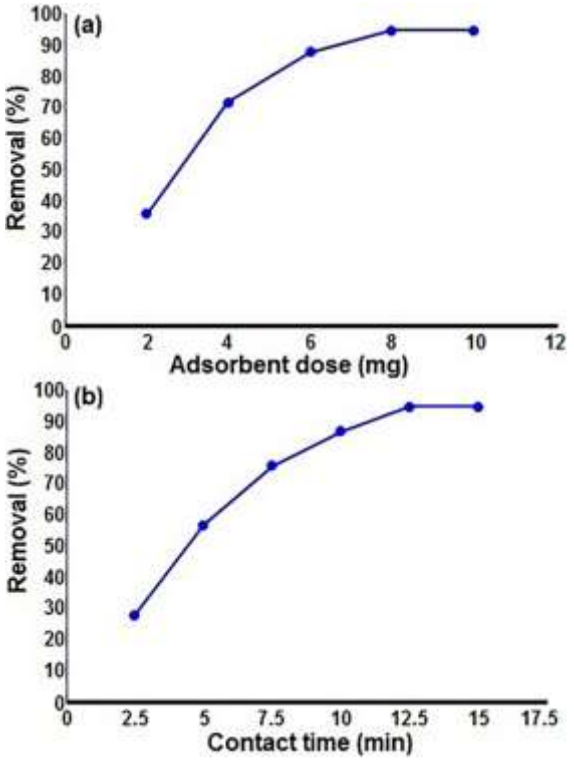

Figure 6. (a) Effect of adsorbent dosage on the adsorption of metal ions by magnetic Fe_3O_4@SiO_2-EDTA NPs; (b) Effect of contact time on the adsorption of metal ions by Fe_3O_4@SiO_2-EDTA NPs.

3.4. Adsorption isotherms

Adsorption isotherms of Fe_3O_4@SiO_2-EDTA MNPs with Cu(II) were obtained using batch experiments. This process contains the placing 8 mg Fe_3O_4@SiO_2-EDTA in 60-ml polytetrafluoroethylene-lined screw cap glass tubes receiving 50 mL of $Cu(NO_3)_2$ aqueous solutions with initial concentrations ranging from 0.05 to 0.22 mmol/L for Cu(II). The suspensions were then mixed end over end in incubators at 25, 35 and 45 °C for 15 min. After finding the adsorption equilibrium, magnetically separation was applied to detach Fe_3O_4@SiO_2-EDTA MNPs from the reaction media and the residual concentrations of metal ions were determined by an ICP analyzer. The equilibrium adsorbed concentration, q_e, was calculated according to the equation **(1)**:

$$q_e = \frac{(C_0 - C_e)V}{M} \quad \textbf{(1)}$$

where C_0 (mmol/L) is the initial concentration of Cu(II) ion, C_e (mmol/L) is the equilibrium concentration in solution, V (L) is the total volume of solution, and M (g) is the sorbent mass.

Adsorption isotherms of Cu(II) ions at 25, 35, and 45 °C are shown in Fig 7 in which the equilibrium adsorption capacity of ions decreased directly with temperature. This fact indicates the exothermic process of adsorption.

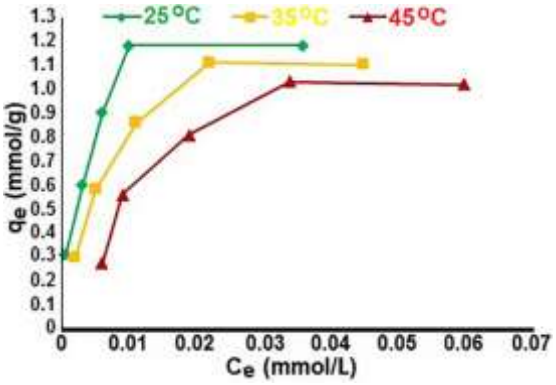

Figure 7. Effect of temperature onto metal ions removal by Fe3O4@SiO2-EDTA MNPs adsorbent.

Table 1 shows a comparison of the adsorbent capacity of various adsorbents for Cu(II) metal ions. The variation in maximum adsorption capacities between the adsorbents could be related to the type and concentration of surface groups responsible for adsorption of metal ions from the solution. By comparison, the novel Fe_3O_4@SiO_2-EDTA prepared here show fast adsorption and high adsorption capacity.

Table 1. Comparison of maximum adsorption capacities of different adsorbents for removal of Cu(II) metal ions.

Adsorbents	Maximum adsorbed amount, q_m (mg/g)	Ref.
Iron oxide NPs	19.3	[37]
Multi-amine-grafted mesoporous silicas	1.0	[38]
MWCNTs–IDA	6.6	[39]
Purolite Arsen X^{np}	5.57	[40]
magnetite nanorods	40	[41]
dairy manure biochar	54.4	[42]
iron oxide coated sewage sludge	17.3	[43]
iron oxide nanoparticles-immobilized-sand	5.81	[44]
activated charcoal derived from coffe	38.2	[45]
Fe_3O_4@SiO_2- EDTA NPs	**75.4**	**This work**

3.5. Effect of adsorbent on the effluent of Songun copper processing plant

The effluent sample of Songun copper processing plant was simulated and artificially prepared in the laboratory and used in this research. Results of ICP analysis of element concentrations in the effluent of Songun copper plant is given in **Table 2**.

Table 2. Concentration of heavy metals in the effluent of Songun processing plant.

Metal ion	Metal Concentration (mg/L)	Permissible concentration in the effluent (mg/L)	Permissible concentration in drinking water (mg/L)
Cd	0.05>	1	0.003
As	>0.05	0.1	0.01
Cr	0.34	0.5	0.05
Pb	0.27	0.1	0.01
Cu	44.48	1	0.1
Ni	0.88	2	0.02
Ag	>0.05	1	0.05
Zn	3.04	2	0.2

Due to the fact that the amounts of heavy metals copper, lead and zinc in the effluent are higher than the standard limit, the amount of adsorption of these elements after the addition of adsorbent was investigated, the results are summarized in the **Table 3**.

Table 3. The rate of metal ion adsorption in the simulated effluent in the presence of Fe_3O_4@SiO_2-EDTA nanosorbent.

Metal ion	Metal Concentration (mg/L)	Metal Concentration (mmol/L)	Adsorbed (mmol/L)	Removal (%)
Cu	44.48	0.700472	0.609411	87
Pb	0.27	0.001303	0.000195	15
Cd	0.05	0.000445	-	
As	0.05	0.000668	-	-
Cr	0.34	0.006538	0.001962	30
Ni	0.88	0.014991	0.003898	26
Ag	0.05	0.000463	-	-
Zn	3.04	0.046483	0.019523	42

The results indicate that the addition of 35 mg of adsorbent to the prepared 50 ml solution will lead to the absorption of 85%, 15%, 30% and 42% of copper, lead, chromium, nickel and zinc respectively which shows an excellent adsorption and selectivity regarding the copper ions.

3.6. Reusability

The reusability of adsorbents after a particular process is one of the most important properties for environmental and economic reasons [46-48]. Also, two interesting privileges these kinds of adsorbents are higher adsorption capability as well as better desorption property which reduce the overall cost of adsorbent. Having magnetic properties, the collection of was very easy and quick. It seems that acid treatment metal-adsorbed Fe_3O_4@SiO_2-EDTA is a feasible manner for desorption of copper ions loaded adsorbent at low pH. Therefore, the desorption of Cu(Π) ions was carried out by HCl (1 mol/L) at 25°C, and the results are shown in **Figure. 8**. According to these results, it can be seen a bit loss in adsorption capacity after six consecutive adsorption-desorption cycles, indicating the good performance and recyclability of the prepared Fe_3O_4@SiO_2-EDTA without noticeably decreasing in activity.

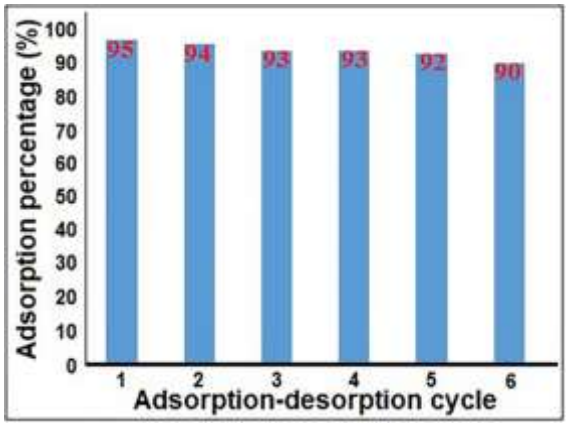

Figure 8. (a) Adsorption efficiency of Cu(II) in the adsorption-desorption cycles by Fe_3O_4@SiO_2-EDTA MNPs at 25 ºC.

4. Conclusion

A novel magnetic nano-adsorbent containing Fe_3O_4 nanoparticles functionalized with EDTA was fabricated and exhibited remarkable enhancement of Cu(II) removal efficiency from aqueous solutions. The sorption conditions for the sorbent were optimized by varying several experimental parameters such as adsorption contact time, effect of adsorbent dosage and sorbate concentration. Fe_3O_4@SiO_2-EDTA MNPs provides numerous surface hydroxyl and triazine nitrogen groups on the MNPs, which provide a strong affinity for copper ions with easy magnetic separation, and the maximal adsorption. Therefore, simple preparation procedure, great adsorption capacity, fast adsorption speed and good reusability make the nanocomposite an environmentally friendly and economically viable adsorbent for rapid removal of heavy metal ions from polluted water.

Acknowledgments

We are grateful to Payame Noor University for its financial support.

References

[1] M. Chiban, A. Soudani, F. Sinan and M. Persin, *Colloids. Surf* **82** (2011) 267.

[2] A. Moghimi and M. Abniki, *J. Color. Sci. Tech* (2021) JCST-2012-1121.

[3] M. Abniki and A. Moghimi, Micro & Nano Letters **16** (2021) 455.

[4] P. Rudnicki, Z. Hubicki and D. Kołodynska, *Chem. Eng. J* **252** (2014) 362.

[5] Y. Guo, H. Guo, Y. Wang, L. Liu and W. Chen, *RSC Adv* **4** (2014) 14048.

[6] J. Mukherjee, D. P. Dutta, J. Ramakumar and A.K. Tyagi, *J. Environ. Chem. Eng* **4** (2016) 3050.

[7] N. Zhang, G.L. Zang, C. Shi, H.Q. Yu and G.P. Sheng, *J. Hazard. Mater* **316** (2016) 11.

[8] I. Luo, X. Lei, X. Xie, B. Yu, N. Cai and F. Yu, *Carbohydr. Polym* **151** (2016) 640.

[9] W. S. Wan Ngah, L. C. Teong and M. A. K. M. Hanafiah, *Carbohyd. Polym* **83** (2011) 1446.

[10] D. Kołodynska, M. Kowalczyk and Z. Hubicki, *J. Mater. Sci* **49** (2014) 2483.

[11] R.A.K. Rao and M.A. Khan, *Sep. Purif. Technol* **57** (2007) 394.

[12] S. Yang, L. Wang, S. Yue, X. Guo, Y. Song and J. He, *RSC Adv* **3** (2013) 16990.

[13] M. A. Khan, W. Jung, O.H. Kwon, Y.M. Jung, K.J. Paeng, S.Y. Cho and B.H. Jeon, *J. Ind. Eng. Chem* **20** (2014) 4353.

[14] J. Gallo, N. Kamaly, I. Lavdas, E. Stevens, Q. D. Nguyen, M. Wylezinska-Arridge, E. O. Aboagye and N. J. Long, *Angew. Chem., Int. Ed* **53** (2014) 9550.

[15] M. Esmaeilpour, A. R. Sardarian and H. Firouzabadi, *Chemistry. Select* **3** (2018) 9236.

[16] J. S. Hu, L. S. Zhong, W. G. Song and L. J. Wan, *Adv. Mater* **20** (2008) 2977.

[17] M. Kazemnejadi, S. A. Alavi, Z. Rezazadeh, M. A. Nasseri, A. Allahresani and M. Esmaeilpour, *J. Mol. Struct* **1186** (2019) 230.

[18] M. Esmaeilpour, A. R. Sardarian and H. Firouzabadi, *J. Appl. Organomet. Chem* **873** (2018) 22.

[19] L. Rodriguez-Arco, I. A. Rodriguez, V. Carriel, A. B. Bonhome Espinosa, F. Campos, P.

Kuzhir, J. D. G. Duran and M. T. Lopez-Lopez, *Nanoscale* **8** (2016) 8138.

[20] S. Zahmatkesh, M. Esmaeilpour and J. Javidi, *RSC. Adv* **6** (2016) 90154.

[21] I. Dindarloo Inaloo, S. Majnooni, H. Eslahi and M. Esmaeilpour, *Mol. Catal* **492** (2020) 110915.

[22] Y. Zhao, Q. Zumin and J. Huang, *Chin. J. Chem. Eng* **16** (2008) 451.

[23] M. Esmaeilpour, J. Javidi and M. Zandi, *Mater. Res. Bull* **55** (2014) 78.

[24] M. Esmaeilpour, A. R. Sardarian, A. Jarrahpour and E. Ebrahimi, J. Javidi, *RSC Adv* **6** (2016) 43376.

[25] R. Xiong, Y. Wang, X. Zhang, C. Lu and L. Lan, *RSC Adv* **4** (2014) 6454.

[26] J. Javidi, M. Esmaeilpour and M. Rajabnia Khansari, *RSC Adv* **5** (2015) 73268.

[27] M. Esmaeilpour, A. R. Sardarian and H. Firouzabadi, *Appl. Organomet. Chem* (2018) 4300.

[28] A. R. Sardarian, M. Kazemnejadi and M. Esmaeilpour, *Dalton Trans* **48** (2019) 3132.

[29] M. Esmaeilpour, S. Zahmatkesh, N. Fahimi and M. Nosratabadi, *Appl Organometal Chem* (2018) 4302.

[30] I. Dindarloo Inaloo, S. Majnooni and M. Esmaeilpour, *Eur. J. Org. Chem* (2018) 3481.

[31] M. Esmaeilpour, J. Javidi, F. Nowroozi Dodeji and M. Mokhtari Abarghoui, *J. Mol. Catal A: Chem* **393** (2014) 18.

[32] M. Ghiaci, M. Zarghani, F. Moeinpour and A. Khojastehnezhad, *Appl. Organomet. Chem* **28** (2014) 589.

[33] I. Dindarloo Inaloo, S. Majnooni, H. Eslahi and M. Esmaeilpour, *ACS Omega* **5** (2020) 7406.

[34] A. R. Sardarian, H. Eslahi and M. Esmaeilpour, *ChemistrySelect* **3** (2018) 1499.

[35] I. Dindarloo Inaloo, S. Majnooni, H. Eslahi and M. Esmaeilpour, *Appl. Organomet. Chem* (2020) e5662.

[36] J. Javidi and M. Esmaeilpour, *Mater. Res. Bull* **73** (2016) 409.

[37] S. S. Banerjee and D. H. Chen, *J. Hazard. Mater* **147** (2007) 792.

[38] L. Zhang, C. Yu. W. Zhao, Z. Hua, H. Chen, L. Li and J. Shi, *J. Non-Cryst. Solids* **353** (2007) 4055.

[39] J. Wang, X. Ma, G. Fang, M. Pan, X. Ye and S. Wang, *J. Hazard. Mater* **186** (2011) 1985.

[40] D. Kołodyńska, M. Kowalczyk and Z. Hubicki, *J. Mater.Sci* **49** (2014) 2483.

[41] H. Karami, *Chem. Eng. J.* **219** (2013) 209.

[42] X. Xu, X. Cao, L. Zhao, H. Wang, H. Yu and B. Gao, *Environ. Sci. Pollut. Res* **20** (2013) 358.

[43] T. Phuengprasop, J. Sittiwong and F. Unob, *J. Hazard. Mater* **186** (2011) 502.

[44] S. M. Lee, C. Laldawngliana and D. Tiwari, *Chem. Eng J* **195** (2012) 103.

P. T. Yeung, P. Y. Chung, H. C. Tsang, J. C. O. Tang, G. Y. M. Cheng, R. Gambari, C. H. Chui and K.H. Lam, *RSC Adv* **4** (2014) 38839.

[45] K. Faeze, A. Seyed Naser, R. Bibi Marziyeh, *J. Of Applied Chemistry*, **16** (1400) 59, in Persian.

[46] E. Mohammad, E. Shahla, *J. Of Applied Chemistry*, **16** (1400) 58, in Persian.

[47] E. Homeira, K. Saees, A. Aliakbar, M. Zahra, *J. Of Applied Chemistry*, **15** (1399) 55, in Persian.